ELSEVIER

Journal of Hazardous Materials B136 (2006) 632–644

Journal of Hazardous Materials

www.elsevier.com/locate/jhazmat

Photo-assisted Fenton type processes for the degradation of phenol: A kinetic study

Hrvoje Kušić, Natalija Koprivanac *, Ana Lončaric Božić, Iva Selanec

University of Zagreb, Faculty of Chemical Engineering and Technology, Marulićev Trg 19, HR-10000, Zagreb, Croatia

Received 12 July 2005; received in revised form 14 November 2005; accepted 22 December 2005
Available online 8 February 2006

Abstract

In this study the application of advanced oxidation processes (AOPs), dark Fenton and photo-assisted Fenton type processes; Fe^{2+}/H_2O_2, Fe^{3+}/H_2O_2, Fe^0/H_2O_2, $UV/Fe^{2+}/H_2O_2$, $UV/Fe^{3+}/H_2O_2$ and $UV/Fe^0/H_2O_2$, for degradation of phenol as a model organic pollutant in the wastewater was investigated. A detail kinetic modeling which describes the degradation of phenol was performed. Mathematical models which predict phenol decomposition and formation of primary oxidation by-products: catechol, hydroquinone and benzoquinone, by applied processes were developed. The study also consist the modeling of mineralization kinetic of the phenol solution by applied AOPs. This part, besides well known reactions of Fenton and photo-Fenton chemistry, involves additional reactions which describe removal of iron from catalytic cycle through formation of ferric complexes and its regeneration induced by UV radiation. Phenol decomposition kinetic was monitored by HPLC analysis and total organic carbon content measurements (TOC). Complete phenol removal was obtained by all applied processes. Residual TOC by applied Fenton type processes ranged between 60.2 and 44.7%, while the efficiency of those processes was significantly enhanced in the presence of UV light, where residual TOC ranged between 15.2 and 2.4%.

Keywords: Photo-Fenton reaction; UV radiation; Wastewater; Phenol; Kinetic modeling

1. Introduction

Phenols occupy a prominent place among the pollutants of ground waters [1]. A large part of that pollution is caused by industry. Due to the wide utilization in different industries, e.g. chemical, petrochemical, paint, textile, pesticide plants, etc., phenols have become the most abundant pollutants in industrial wastewater. They serve as intermediates in the industrial synthesis of products as diverse as adhesives and antiseptics are [2]. Their presence contributes notably to the pollution of the effluents due to their high toxicity to aquatic life, and may cause carcinogenic and mutagenic effects to humans [3]. Common commercial wastewater treatment methods utilize the combination of biological, physical and chemical treatment [4,5]. Biotreatment processes tend to be very large due to the slow rate of the biological reactions [5]. Furthermore, physical methods for wastewater treatment do not involve chemical transformations, and generally transfer waste components from one phase to another. Chemical treatment of phenols, such as chlorination, can result with formation of chlorinated phenols and their by-products which are reported as toxic and nonbiodegradable [6].

An attractive alternative for the treatment of toxic organic contaminants present in wastewater, including phenols, are so-called advanced oxidation processes (AOPs) which generate hydroxyl radicals in sufficient quantities for oxidizing the majority of the organics present in the effluent water [7–10]. Common AOPs involve Fenton and Fenton "like" processes, ozonation, photochemical and electrochemical oxidation, photolysis with H_2O_2 and O_3, high voltage electrical discharge (corona) process, TiO_2 photocatalysis, radiolysis, water solutions treatment by electronic beams or γ-beams and various combinations of these methods [8–10]. The mostly used AOPs are Fenton type processes. The primary benefits of Fenton type processes are their ability to convert a broad range of pollutants to harmless or biodegradable products and the fact that their relatively cheap reagents are safe to handle and are environmentally benign [11]. The degradation of organic pollutants by Fenton type processes could be significantly accelerated in the presence of UV light

* Corresponding author. Tel.: +385 1 4597 124; fax: +385 1 4597 143.
E-mail address: nkopri@marie.fkit.hr (N. Koprivanac).

0304-3894/$ – see front matter © 2006 Elsevier B.V. All rights reserved.
doi:10.1016/j.jhazmat.2005.12.046

irradiation, resulting with complete mineralization of organic pollutants [12].

In the present work investigations were directed to find the optimal operating parameters of applied dark Fenton type processes, Fe^{2+}/H_2O_2, Fe^{3+}/H_2O_2 and Fe^0/H_2O_2 for the degradation of phenol as a model organic pollutant in the wastewater. Furthermore, the efficiency of dark Fenton and photo-assisted Fenton type processes; Fe^{2+}/H_2O_2, Fe^{3+}/H_2O_2, Fe^0/H_2O_2, $UV/Fe^{2+}/H_2O_2$, $UV/Fe^{3+}/H_2O_2$ and $UV/Fe^0/H_2O_2$, at established optimal conditions for each process was studied. The principal objective was to perform a detail kinetic modeling which describes degradation of phenol by applied AOPs. The experiments were focused on the measurement of phenol and primary oxidation by-products decay as well as on the mineralization of the phenol solution by applied processes. The mathematical modeling was performed in order to predict phenol decomposition and profiles of catechol, hydroquinone and benzoquinone, as well as mineralization of the phenol solution by all applied processes. These processes include Fenton type and auxiliary processes: UV radiation process, UV radiation combined with addition of ferrous and ferric salts and iron powder and UV/H_2O_2 process. For all cases, developed mathematical models are solved numerically and compared to the experimental data.

2. Experimental

Chemicals used in this study were supplied by Fluka, Germany (phenol, catechol, hydroquinone, benzoquinone, acetonitrile and acetic acid) and Kemika, Croatia ($FeSO_4{\cdot}7H_2O$, $Fe_2(SO_4)_3{\cdot}9H_2O$, iron powder, H_2O_2, 30%, sulfuric acid, >95%). All solutions were prepared with deionized water with conductivity less than 1 μScm^{-1}. The concentration of model phenol solution was 0.1 gL^{-1}.

The set of preliminary experiments was conducted in order to establish the optimal ratio of Fenton reagent in Fe^{2+}/H_2O_2, Fe^{3+}/H_2O_2 and Fe^0/H_2O_2 processes at initial concentration of iron catalyst 0.5 and 1 mM. Ferrous and ferric sulphates, $FeSO_4{\cdot}7H_2O$ and $Fe_2(SO_4)_3{\cdot}9H_2O$, and iron powder, were used as a source of iron in applied Fenton type processes. The concentration of hydrogen peroxide was varied to give molar ratios 1:5, 10, 20, 30, 40, 50, 60, 70, 80, 90, 100, i.e. until the achievement of the maximal mineralization extent. Concerning knowledge from the literature which reports the usage of Fenton process for the treatment of phenol wastewater [12–16], at the beginning of all experiments pH was adjusted at 3 using 25% sulfuric acid, which was followed by addition of Fenton reagent. Reaction mixture ($V = 250$ mL) was continuously stirred at room temperature in an open batch system with magnetic stirring bar and treated for 1 h, while TOC values were measured at the end of each experiment in order to establish mineralization extents.

Experiments at established optimal conditions with the highest mineralization extents for each Fenton type process were repeated in the absence and in the presence of UV light radiation, in order to determine phenol degradation kinetics. All further experiments were performed in the glass water-jacketed batch reactor (180 mm long, 75 mm diameter) with a capacity of 0.8 L (Fig. 1). A quartz tube was placed vertically in the middle of the reactor. The tube contained a mercury lamp 125 W (UV-C, 254 nm), UVP—Ultra Violet Products, Cambridge, UK and supplied by Hach Company, Loveland, CO, USA. The UV lamp was attached to a power supply, UVP—Ultra Violet Products, Upland, CA, USA, with the frequency of 50/60 Hz, $U = 230$ V, $I = 0.21$ A. In experiments where UV radiation was required, $UV/Fe^{2+}/H_2O_2$, $UV/Fe^{3+}/H_2O_2$ and $UV/Fe^0/H_2O_2$, as well as UV, UV/iron catalysts and UV/H_2O_2, the UV lamp was switched on. The value of incident photon flux by reactor volume unit at 254 nm, $I_0 = 3.42 \times 10^{-6}$ Einstein L^{-1} s^{-1}, was calculated on the bases of the ferrioxalate actinometry measurements [17]. The total volume of the treated solutions was 0.5 L in all cases, while the mixing of the solution was provided by both the magnetic stirring bar and the peristaltic pump at a flow rate of 0.1 L min^{-1}. Experiments were carried out at room temperature (25 ± 0.2 °C). The duration of each experiment was 60 min. Samples were taken periodically from the reactor (2, 5, 10, 15, 30, 45 and 60 min) and thereafter immediately analyzed. All experiments were repeated at least two times and averages are reported, while reproducibility of the experiments was within 5%.

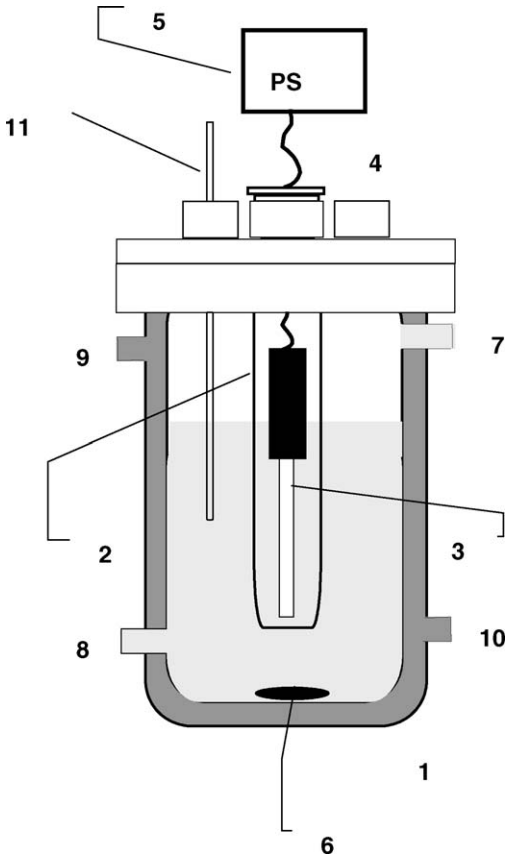

Fig. 1. Schematic diagram of experimental set-up for applied AOPs. (1) glass water-jacketed reactor, (2) quartz jacket, (3) UV lamp, (4) sampling port, (5) power supply, (6) magnetic stirring bar, (7) and (8) solution inlet and outlet, (9) and (10) cooling water inlet and outlet, and (11) thermometer.

The decomposition of phenol (PH) and the formation of primary oxidation by-products: catechol (CC), hydroquinone (HQ) and benzoquinone (BQ), were analyzed by HPLC equipped with Software ClassVP, Shimadzu, Japan, using a 5 μm,

25.0 cm × 4.6 mm, Supelco Discovery C18 column, USA, and detected with diode array UV detector, SPD-M10A$_{VP}$, Shimadzu, Japan. The mobile phase was 2% acetic acid/20% acetonitrile/78% water at 1.0 mL min^{-1}. Phenol decomposition was monitored at $\lambda = 270$ nm ($t_R = 10.05$ min), while the monitoring of formation and then the degradation of by-products were performed at $\lambda = 276$ nm for catechol ($t_R = 5.76$ min), at $\lambda = 290$ nm for hydroquinone ($t_R = 3.97$ min) and at $\lambda = 245$ nm for benzoquinone ($t_R = 5.38$ min). The recorded peaks were first identified and then the concentrations of residual phenol and its formed primary oxidation by-products were determined from their calibration standards. Residual phenol

Table 1
The reactions, rate constants and quantum yields used for the kinetic modeling

#	Reaction	Reference	k ($M^{-1}\,s^{-1}$)	
			Literature	Used
1	$Fe^{2+} + H_2O_2 \rightarrow Fe^{3+} + OH^\bullet$	[15,16,19–23]	63–76	76
2	$Fe^{3+} + H_2O_2 \rightarrow Fe^{2+} + H^+ + HO_2^\bullet$	[15,16,19–23]	0.01–0.02	0.02
3	$Fe^{2+} + OH^\bullet \rightarrow Fe^{3+} + OH^-$	[15,16,19–22]	$(3.0–4.3) \times 10^8$	3.2×10^8
4	$Fe^{3+} + HO_2^\bullet \rightarrow Fe^{2+} + O_2 + H^+$	[15,16,20–22]	$(0.1–3.1) \times 10^5$	3.1×10^5
5	$Fe^{2+} + HO_2^\bullet \rightarrow Fe^{3+} + HO_2^-$	[15,16,20–22]	1.2×10^6	1.2×10^6
6	$Fe^{3+} + O_2^{\bullet-} \rightarrow Fe^{2+} + O_2$	[15,16,19–22]	$(0.5–1.5) \times 10^8$	5.0×10^7
7	$Fe^{2+} + O_2^{\bullet-} \rightarrow Fe^{3+} + H_2O_2$	[15,16,19–22]	1.0×10^7	1.0×10^7
8	$OH^\bullet + H_2O_2 \rightarrow HO_2^\bullet + H_2O$	[15,16,19–22]	$(1.2–4.5) \times 10^7$	4.5×10^7
9	$2OH^\bullet \rightarrow H_2O_2$	[16,19–22]	$(4.2–5.3) \times 10^9$	5.3×10^9
10	$HO_2^\bullet + OH^\bullet \rightarrow H_2O + O_2$	[16,19–23]	6.6×10^{11}	6.6×10^{11}
11	$2HO_2^\bullet \rightarrow H_2O_2 + O_2$	[15,16,19–22]	8.3×10^5	8.3×10^5
12	$O2^{\bullet-} + HO_2^\bullet \rightarrow HO_2^- + O_2$	[15,16,19–22]	9.7×10^7	9.7×10^7
13	$O_2^{\bullet-} + HO^\bullet \rightarrow HO^- + O_2$	[16,20–22]	1.0×10^{10}	1×10^{10}
14	$HO_2^\bullet \rightarrow O_2^{\bullet-} + 2H^+$	[15,16,19–22]	$(1.58–7.9) \times 10^5\ s^{-1}$	$1.58 \times 10^5\ s^{-1}$
15	$O_2^{\bullet-} + 2H^+ \rightarrow HO_2^\bullet$	[15,16,20–22]	1.0×10^{10}	1.0×10^{10}
16	$OH^\bullet + H_2O_2 \rightarrow O_2^{\bullet-} + H_2O$	[16,21,22]	2.7×10^7	2.7×10^7
17	$Fe^0 + H_2O_2 \rightarrow Fe^{2+}$-surface			3.83×10^{-2}
18	Fe^{2+}-surface $+ H_2O_2 \rightarrow Fe^{3+} + OH^\bullet$			6×10^{-2}
19	$Fe^0 + H_2O_2 \rightarrow Fe^{2+} + OH^-$	[23]	0.44–0.23 (pH dep)	1×10^{-2}
20	$H_2O_2 + h\nu \rightarrow 2OH^\bullet$	[15,24,25]		$4.13 \times 10^{-5}\ s^{-1}$
21	$OH^\bullet + HO_2^- \rightarrow HO_2^\bullet + OH^-$	[21,22,24]	7.5×10^9	7.5×10^9
22	$HO_2^\bullet + H_2O_2 \rightarrow H_2O + HO^\bullet + O_2$	[24]	3.0	3.0
23	$O_2^{\bullet-} + H_2O_2 \rightarrow OH^- + HO^\bullet + O_2$	[24]	0.13	0.13
24	$Fe^{3+} + H_2O + h\nu \rightarrow Fe^{2+} + OH^\bullet + H^+$	[11–13,15,26]		3.33×10^{-6}
25	$PH + OH^\bullet \rightarrow DIHCHD^\bullet$	[15,21,22]	*o*: 7.3×10^9	7.3×10^9
26	$DHCD^\bullet + H^+ \rightarrow PH^\bullet + H_2O$	[15,21,22]	5×10^8	5×10^8
27	$DHCD^\bullet + O_2 \rightarrow CC + HO_2^\bullet$	[15,21,22]	1.5×10^9	1.5×10^9
28	$DHCD^\bullet + O_2 \rightarrow HQ + HO_2^\bullet$	[15,21,22]	5.0×10^8	5.0×10^8
29	$DHCD^\bullet + O_2 \rightarrow BQ + HO_2^\bullet$	[15,21,22]	5.0×10^8	5.0×10^8
30	$DHCD^\bullet + BQ \rightarrow PH^\bullet + CC + HQ$	[15,21,22]	3.7×10^9	3.7×10^9
31	$2DHCD^\bullet \rightarrow PH + CC + HC$	[15,21,22]	5.0×10^8	5.0×10^8
32	$2DHCD^\bullet \rightarrow$ products	[15,21,22]	5.0×10^8	5.0×10^8
33	$DHCD^\bullet + PH^\bullet \rightarrow$ products	[15,21,22]	5.0×10^8	5.0×10^8
34	$DHCD^\bullet + PH^\bullet \rightarrow PH + CC + HQ$	[15,21,22]	5.0×10^8	5.0×10^8
35	$PH^\bullet + PH^\bullet \rightarrow$ products	[15,21,22]	1.0×10^9	1.0×10^9
36	$BQ + O_2^{\bullet-} \rightarrow HPH^\bullet + O_2$	[15,21,22]	1.0×10^9	1.0×10^9
37	$CC + OH^\bullet \rightarrow$ products	[21,22]	1.1×10^{10}	1.1×10^{10}
38	$HQ + OH^\bullet \rightarrow$ products	[21,22]	5.0×10^9	5.0×10^9
39	$BQ + OH^\bullet \rightarrow$ products	[21,22]	1.2×10^9	1.2×10^9
40	$PH^\bullet + Fe^{2+} \rightarrow PH + Fe^{3+}$	[15,21,22]	1.0×10^5	1.0×10^5
41	$PH + Fe^{3+} \rightarrow HPH^\bullet + Fe^{2+}$	[15,21,22]	4.4×10^2	4.4×10^2
42	$HPH^\bullet + Fe^{2+} \rightarrow PH + Fe^{3+}$	[15,21,22]	1.1×10^3	1.1×10^3
43	$HPH^\bullet + Fe^{3+} \rightarrow BQ + Fe^{2+}$	[15,21,22]	4.4×10^4	4.4×10^4
44	$BQ + Fe^{2+} \rightarrow HPH^\bullet + Fe^{3+}$	[15,21,22]	1.2×10^{-3}	1.2×10^{-3}
45	$PH + h\nu \Leftrightarrow PH^* \rightarrow CC$			$\Phi = 2.5$ mmol Einstein^{-1}
46	$PH + h\nu \Leftrightarrow PH^* \rightarrow$ products	[25–27]	$\Phi = 11–8$ mmol Ein^{-1}	$\Phi = 17$ mmol Einstein^{-1}
47	$(1-\alpha)\ OC + OH^\bullet \rightarrow IP$			2.33×10^8
48	$Fe^{3+} + \alpha\ OC \rightarrow Fe^{3+}$-complexes	[16]	1.0	1.0
49	Fe^{3+}-complexes $+ h\nu \rightarrow Fe^{3+} + \alpha\ OC$			$1 \times 10^{-3}\ s^{-1}$
50	$OC + h\nu \Leftrightarrow OC^* \rightarrow IP$			$\Phi = 17$ mmol Einstein^{-1}

PH: phenol, DHCD$^\bullet$: dihydroxycyclohexacienyl radical, PH$^\bullet$: phenyl radical, HPH$^\bullet$: hydroxyphenyl radical, CC: catechol, HQ: hydroquinone, BQ: benzoquinone, OC: organic content, IP: inorganic products, and α: fraction of organic content that takes part in Fe scavenging.
* Excited state.

was reported as a normalized value, [phenol]/[phenol]$_{initial}$, while catechol, hydroquinone and benzoquinone formation were reported relative to initial phenol concentration, [catechol]/[phenol]$_{initial}$, [hydroquinone]/[phenol]$_{initial}$, [benzoquinone]/[phenol]$_{initial}$. The mineralization of the phenol solution was established on the basis of total organic carbon content measurements (TOC), performed by total organic carbon analyzer; TOC-V$_{CPN}$ 5000 A, Shimadzu, Japan, and expressed as normalized value of residual organic content [TOC]/[TOC]$_{initial}$. Besides the investigation of phenol degradation by HPLC and TOC measurements, concentrations of iron ions in the bulk during the treatment by applied processes were monitored by colorimetric methods using the UV/Vis spectrophotometer, Lambda EZ 201, Perkin-Elmer, USA. Ferrous ions were identified by the reaction of Fe^{2+} with 1,10-phenanthroline giving orange-red complex (λ_{max} = 510 nm), while ferric ions were determined by the reaction of Fe^{3+} with thiocyanate forming under acidic conditions a red-colored complex (λ_{max} = 480 nm) [18]. Also, the consumption of hydrogen peroxide in the bulk during the treatment by applied processes was monitored using modified iodometric titration method [18].

3. Model formulation

The proposed mathematical models which predict phenol decomposition and formation of primary oxidation by-products: catechol, hydroquinone and benzoquinone, as well as mineralization of the phenol solution by applied AOPs; Fe^{2+}/H_2O_2, Fe^{3+}/H_2O_2, Fe^0/H_2O_2, $UV/Fe^{2+}/H_2O_2$, $UV/Fe^{3+}/H_2O_2$ and $UV/Fe^0/H_2O_2$, were developed using chemical reactions and rate constants, mostly from the literature [15,16,19–27], listed in the Table 1. The number of chemical species and chemical reactions included in each model varied in dependence with specific AOP and the analytical method used for monitoring of phenol degradation (Table 2). The general mass balance for a well-mixed, constant volume and constant temperature batch reactor is given by

$$dc_i/dt = -r_i \quad (1)$$

where c_i is concentration of specie i in the bulk and r_i is the bulk phase rate of the same specie [28]. Phenol degradation was simulated by Mathematica 5.0 (Wolfram Research, Champaigne, IL) using GEAR method which finds the numerical solution to the set of ordinary differential equations. Values of rate constants of reactions, 17–20, 24, 47 and 49, and quantum yield, 45 (Table 1) were determined by trial and error method fitting the values into the models 2, 4, 5, 8, 10 and 12 (Table 2). Models 1 and 2 describing Fenton mechanism were considered as basic. The model 1 was developed strictly by using the values from the literature for the proposed reactions (Tables 1 and 2). In the model 2, which describes basic Fenton process for the mineralization of organic pollutant, the value of rate constant for reaction 47 was determined and subsequently used for the developing model 4. In the model 4, the values of rate constants for reaction 17–19 were determined and subsequently used in further modeling for the model 3. Further modeling was done in order to establish the value of quantum yield of catechol in the model 5. Using earlier specified value of rate constant for the reaction 47 from the model 2, the value of rate constant for the reaction 24 was determined in the model 8, as well as the value of rate constant for the reaction 20 in the model 10. At the end, the value of rate constant for the reaction 49 was determined by including all earlier specified values of rate constants for the reactions 20, 24 and 47 into the model 12.

Table 2
The list of developed AOP models concerning source of experimental data and used reactions

Model #	AOP	Exp. data source	Reaction # (Table 1)
1	Fe^{2+}/H_2O_2 & Fe^{3+}/H_2O_2	HPLC	1–6, 25–44
2	Fe^{2+}/H_2O_2 & Fe^{3+}/H_2O_2	TOC	1–6, 47, 48
3	Fe^0/H_2O_2	HPLC	1–9, 25–44
4	Fe^0/H_2O_2	TOC	1–9, 47, 48
5	UV	HPLC	45, 46
6	UV	TOC	50
7	UV/Fe^{3+}	HPLC	1–6, 24–46
8	UV/Fe^{3+}	TOC	1–6, 24, 47–50
9	UV/H_2O_2	HPLC	8–16, 20–23, 25–46
10	UV/H_2O_2	TOC	8–16, 20–23, 47, 50
11	$UV/Fe^{2+}/H_2O_2$ & $UV/Fe^{3+}/H_2O_2$	HPLC	1–16, 20–46
12	$UV/Fe^{2+}/H_2O_2$ & $UV/Fe^{3+}/H_2O_2$	TOC	1–16, 20–24, 47–50
13	$UV/Fe^0/H_2O_2$	HPLC	1–46
14	$UV/Fe^0/H_2O_2$	TOC	1–24, 47–50

4. Results and discussion

4.1. Optimization of dark Fenton type processes

The oxidation power of Fenton reagent depends very much on the operating parameters: iron concentration, source of iron catalysts (ferrous or ferric salts, iron powder), H_2O_2 concentration, iron catalyst/hydrogen peroxide ratio, temperature, pH and treatment time [29]. Therefore, it is necessary to find optimal process parameters through laboratory treatability tests. In this work a set of experiments using different source of iron catalyst, iron catalyst concentration and molar ratios of iron catalyst/H_2O_2 were conducted. The goal was to establish optimal values of studied parameters for each Fenton type process at pH 3, the value proposed in the literature for phenol degradation by Fenton process [12–16]. In Fig. 2 obtained values of mineralization degree after performed treatability tests for phenol degradation by studied dark Fenton type processes: (A) Fe^{2+}/H_2O_2, (B) Fe^{3+}/H_2O_2 and (C) Fe^0/H_2O_2 were presented. The experiments were conducted at two initial concentrations of iron catalysts, 0.5 and 1.0 mm, while hydrogen peroxide concentrations were varied to give the iron catalyst/H_2O_2 ratio 1:5, 10, 20, 30, 40, 50, 60, 70, 80, 90, 100, i.e. until maximal mineralization extents were achieved. The highest mineralization extent of phenol solution among applied Fenton type processes, was obtained by Fe^{3+}/H_2O_2 process, 55.3% of removed TOC, at

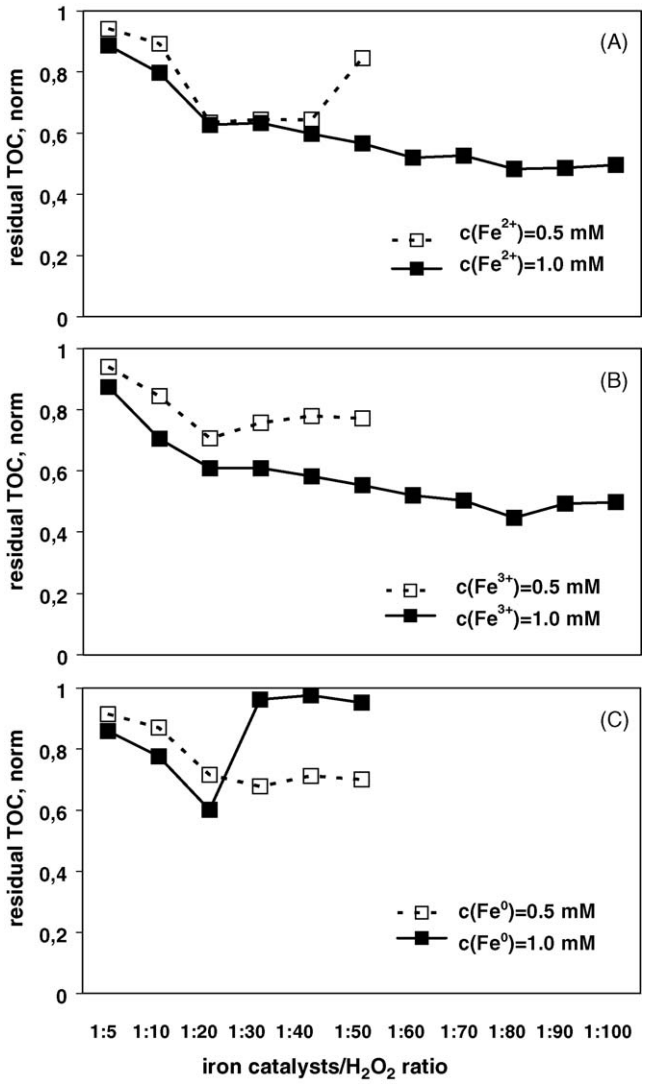

Fig. 2. Influence of iron catalyst concentration and iron catalyst/H_2O_2 ratio on mineralization of phenol solution by Fenton type processes at pH 3; (A) Fe^{2+}/H_2O_2, (B) Fe^{3+}/H_2O_2 and (C) Fe^0/H_2O_2. Lines are only for connecting points and are not model results.

$c(Fe^{3+}) = 1.0$ mM, Fe^{3+}/H_2O_2 ratio 1: 80 at pH 3 (Fig. 2(B)). At the same iron concentration and iron catalyst/hydrogen peroxide ratio 51.8% of removed TOC was achieved by the treatment with Fe^{2+}/H_2O_2 (Fig. 2(A)), while in the case of Fe^0/H_2O_2 process the highest mineralization extent, 39.8% of TOC removal, was obtained with $c(Fe^0) = 1.0$ mM and Fe^0/H_2O_2 ratio 1:20 at pH 3 (Fig. 2(C)). The efficiency of Fenton type processes is influenced by the concentration of Fe^{2+} ions which catalyze hydrogen peroxide decomposition resulting with OH radical production and consequently the degradation of organic molecule. According to the literature [29], a minimal threshold concentration of ferrous ions that allows the reaction to proceed within the reasonable period of time ranges between 3 and 15 mgL^{-1}, regardless of the concentration of organic pollutant. However, iron levels <25–50 $mg\,L^{-1}$ can require excessive reaction times (10–24 h). This is particularly true where the oxidation products (organic acids) sequester the iron and remove it from the catalytic cycle

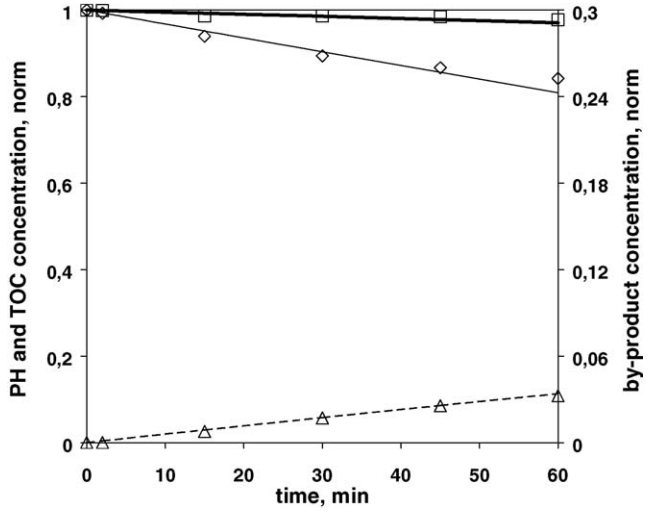

Fig. 3. Treatment of phenol solution by UV process, comparison of experimental data and data predicted by developed mathematical models 5 and 6. Phenol degradation and formation of primary oxidation by-products. Symbols: PH, (ε) exp. and (—) model; TOC, (□) exp. and (▬) model; CC, (△) exp. and (- - -) model.

[29]. In this study iron concentrations of 0.5 and 1.0 mM were used in all three Fenton type processes. Better results in the mineralization of phenol solution were obtained with 1.0 than with 0.5 mM of iron catalysts in all three dark Fenton type processes. Also, with increasing hydrogen peroxide concentration, degradation efficiency was increased to the achievement of certain optimal Fenton reagent ratio. In the cases of Fe^{2+}/H_2O_2 and Fe^{3+}/H_2O_2 processes ratio 1:80 and 1:20 in the case of Fe^0/H_2O_2 process were shown to be the most efficient (Fig. 2(A), (B) and (C)). With further increasing of hydrogen peroxide concentration, phenol degradation efficiency was decreased due to the scavenging nature of hydrogen peroxide towards OH radicals when present in higher concentration. Formed perhydroxyl radicals (Table 1, #8) are significantly less reactive than hydroxyl radicals and thus directly influence the efficiency of organic pollutant degradation [29,30]. It should be emphasized that in the case of Fe^0/H_2O_2 process when the H_2O_2 is in excess, besides scavenging nature of hydrogen peroxide towards OH radicals, an inert oxidative film on the iron powder surface could be created. In that way, the further leaching of Fe^{2+} ions could be disabled resulting in a negative influence of the Fe^0/H_2O_2 process efficiency for organic pollutant degradation [31]. That effect is strongly pronounced at Fe^0/H_2O_2 ratios over 1:20, especially at $c(Fe^0) = 1.0$ mM (Fig. 2(C)).

4.2. UV auxiliary tests

As it was mentioned earlier, in model formulation part, models 1 and 2 which describe phenol degradation by Fenton process were developed as basic models. For further successful development of kinetic models for the prediction of phenol degradation by photo-assisted Fenton type processes, the conduction of the three significant auxiliary test experiments were required. From the first set of experiments necessary to establish efficiency of UV process for phenol degradation (Fig. 3), the quantum yield of

phenol was calculated by inserting the experimentally obtained data into Eq. (2):

$$c_{i0} - c_i - \frac{1}{\xi}\ln\left[\frac{1-\exp(-\xi c_{i0})}{1-\exp(-\xi c_i)} = \Phi_i I_0 t\right] \quad (2)$$

where $\xi = 2.303 \times \varepsilon_i \times L$, and c_i is concentration of specie i in the bulk during the treatment, while c_{i0} presents initial concentration of the same specie. I_0 is the value of incident radiation photon flux by reactor volume unit, L the radiation pathway, ε_i is the molar absorption coefficient of specie i and Φ_i presents quantum yield of the same specie [27]. Once I_0, 3.42×10^{-6} Einstein L^{-1} s^{-1}, and L, 3 cm, are known by actinometry experiments, the quantum yield of the specie i can be calculated. The value of molar absorption coefficient of phenol was calculated from Eq. (3) by measuring absorbance of the phenol solution at 254 nm. The obtained value was in compliance with value reported in the literature, $\varepsilon = 516\ M^{-1}\ cm^{-1}$ [25,27]. Absorbance A can be expressed as:

$$A = \varepsilon \times l \quad (3)$$

where ε is the molar absorption coefficient with dimensions 1/(concentration × length), and l is the cell path length [32]. The calculated value of phenol quantum yield, 0.017 mol Einstein^{-1}, is in the range of the values reported in the literature. Rodríguez et al. [26] reported the value of phenol quantum yield 0.011 ± 0.002 mol Einstein^{-1}, while Gimeno et al. [27] reported 0.018 mol Einstein^{-1}. After determining the value of quantum yield of phenol, models 5 and 6 were developed as semiempirical models based on the Lambert' law, so-called LLmodels [25]. The model 5 describes phenol degradation by UV process to detected primary by-products, in this case only catechol. The quantum yield of catechol, 0.0025 mol Einstein^{-1}, was determined by trial and error method inserting values into the model and comparing calculated data with experimentally obtained data for catechol production. The value of molar absorption coefficient of catechol, $\varepsilon_{CC} = 4070\ M^{-1}\ cm^{-1}$, was obtained by measuring catechol absorbance at 254 nm and calculating ε from Eq. (3). In the developed model 6 which was used for prediction of partial mineralization of phenol solution by UV process, the value of phenol quantum yield was used as the value of quantum yield for the complete organic content of the initial phenol solution. From Fig. 3 a good accordance of experimentally obtained data for phenol decomposition and formation of catechol, as well as partial mineralization of phenol solution, with data predicted by developed mathematical models 5 and 6 can be observed. From the aspect of the effectiveness of UV process for phenol degradation, it can be seen that UV process without addition of any catalysts or oxidants showed very low phenol degradation. Only 15.8% of phenol was degraded whilst 3.2% of catechol was detected and only 2.2% of phenol solution was completely mineralized (Fig. 3). The discrepancy between the amount of degraded phenol and the produced catechol, and on the other side the mineralized part of phenol solution could be contributed to the formation of other by-products, e.g. aliphatic organic acids (HAA) [27,33,34], which can be formed through degradation of aromatic by-products, e.g. catechol. But according to the results presented in Fig. 3, HAA may also be formed by the direct degradation of phenol.

The next important set of auxiliary tests involved the investigation of the UV/Fe^{3+} process for phenol degradation where concentration of ferric ions was 1.0 mM. Models 7 and 8 which predict phenol degradation to the primary by-products, and phenol mineralization, by UV/Fe^{3+} process, were developed. It is well known from the literature [26,35–39] that the presence of ferric ions could enhance UV photolysis of organic pollutants due to the generation of OH radicals via reduction of Fe^{3+} ions under UV irradiation, reaction 24 (Table 1). In this case, both UV photolysis mechanism and degradation of organics throughout OH radical attack should be considered as mechanisms responsible for organic pollutant degradation [25]. Therefore, in order to predict the kinetic of phenol degradation by UV/Fe^{3+} process, besides earlier developed models 5 and 6 which include phenol degradation mechanism by UV photolysis, the degradation of phenol throughout OH radical mechanism should also be included. Thus, models 1 and 2 were upgraded with additional reactions 24, 45 and 46 as well as 24 and 50 (Table 1) to give models 7 and 8, respectively. Although those reactions seem to be the most important in the phenol degradation by UV/Fe^{3+} process, the set of principal inorganic reactions which are considered common to the Fenton reaction system, was also included into models 7 and 8. Reactions 1–7 and 8–16 (Table 1) describe iron oxidation/reduction and radical reactions occurring during the process, respectively. The value of rate constant for the reaction 24, $3.33 \times 10^{-6}\ M^{-1}\ s^{-1}$, was determined by trial and error method fitting the values into model 8 which describes phenol mineralization using earlier determined rate constant for the reaction 47 in model 2, $2.33 \times 10^{8}\ M^{-1}\ s^{-1}$ (Table 1). Furthermore, in model 7 which describes phenol degradation to the primary oxidation by-products, besides so-called Fenton reactions used in model 8, a set of reactions specific for the decomposition of phenol to detected aromatic by-products was included, 25–44 (Table 1). From Fig. 4 a good accordance of experimentally obtained results and those predicted by developed kinetic models 7 and 8 for phenol degradation by UV/Fe^{3+} process (A) and profiles of Fe^{2+}/Fe^{3+} ions during the same process (B) can be observed. From the degradation point of view, it can be seen that the UV process efficiency was significantly enhanced by the presence of Fe^{3+} ions; from 15.8% of degraded phenol by the UV process up to 53.6% by UV/Fe^{3+} process, whilst 14.2% of catechol, 2.6% of hydroquinone and 4.5% of benzoquinone were detected (Fig. 4 (A)). Similar results were obtained by Rodríguez et al. [26] who reported phenol removal after 1 h treatment by UV/Fe^{3+} process in range from 45–60% depending on [Fe^{3+}]/[phenol] ratio. Also, partial mineralization of the phenol solution was promoted by reactions of OH radicals which were generated by the reduction of Fe^{3+} ions in the presence of UV light. Residual TOC decreased from 97.8% to the 90.6% by UV and UV/Fe^{3+} processes, respectively. The formation of phenol by-products such as catechol, hydroquinone and benzoquinone speaks in favor of degradation mechanism throughout OH radicals. These by-products are formed by the oxidation of dihydroxycyclohexadienyl radicals which are direct products of OH radical attack to the phenol molecules, reaction

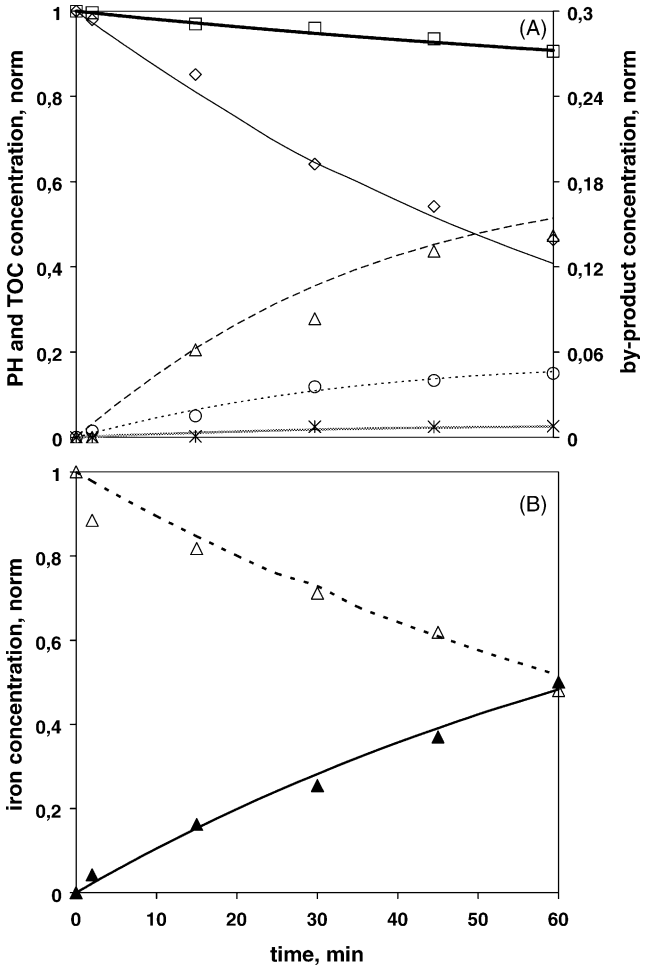

Fig. 4. Treatment of phenol solution by UV/Fe^{3+} process, comparison of experimental data and data predicted by developed mathematical models 7 and 8. (A). Phenol degradation and formation of primary oxidation by-products. Symbols: PH, (◊) exp. and (—) model; TOC, (□) exp. and (▬) model CC, (△) exp. and (- - -) model; HQ, (✳) exp. and (▭) model; BQ, (◯) exp. and (· - · -) model. (B) Profiles of Fe^{2+} and Fe^{3+} ions. Symbols: Fe^{2+}, (▲) exp. and (—) model; Fe^{3+}, (△) exp. and (- -) model.

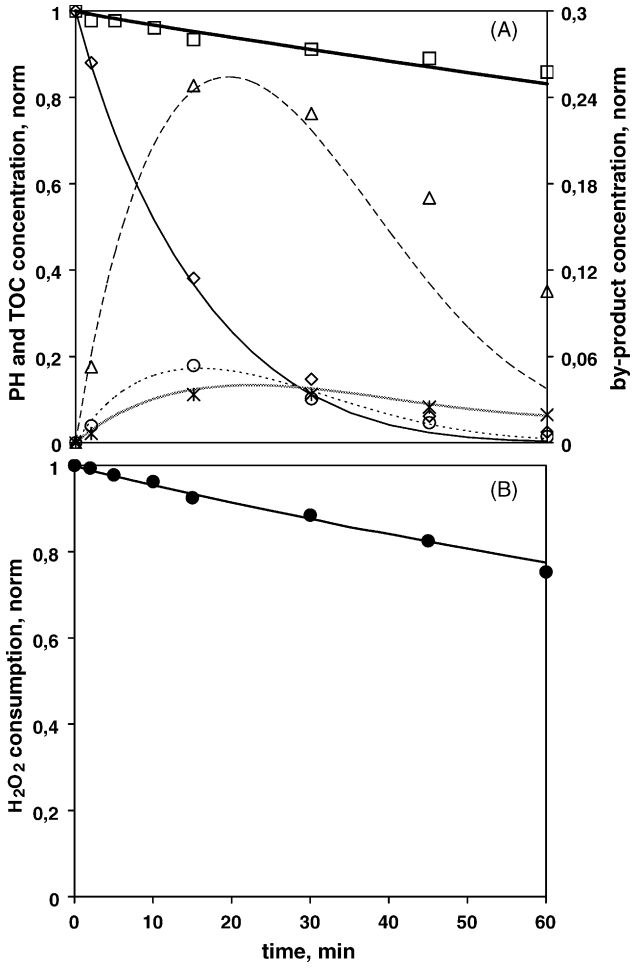

Fig. 5. Treatment of phenol solution by UV/H_2O_2 process, comparison of experimental data and data predicted by developed mathematical models 9 and 10. (A) Phenol degradation and formation of primary oxidation by-products. Symbols: PH, (◊) exp. and (—) model; TOC, (□) exp. and (▬) model CC, (△) exp. and (- - -) model; HQ, (✳) exp. and (▭) model; BQ, (◯) exp. and (· - · -) model. (B) H_2O_2 consumption. Symbols: (●) exp. and (—) model.

25 (Table 1) [15,21,22]. Validity of models 7 and 8 was also confirmed by a good accordance of predicted and experimentally obtained data for the evolution of Fe^{2+} and Fe^{3+} ions in the bulk during the UV/Fe^{3+} process (Fig. 4(B)).

Further set of auxiliary experiments involved phenol degradation by UV/H_2O_2 process, c(H_2O_2) =20 mM, which was done in order to determine the rate of reaction 20 (Table 1), i.e. the reaction of H_2O_2 decomposition to the OH radicals under UV light. For this purpose two additional kinetic models were developed, models 9 and 10. Firstly, model 10 which predicts phenol mineralization by UV/H_2O_2 process using radical reactions in the bulk (8–16), generation of OH radicals due to H_2O_2 decomposition (20), additional bulk radical reactions specific for the UV/H_2O_2 process (21–23), and reactions for degradation of phenol both due to OH radicals and direct photolysis (47 and 50), was developed. The value of rate constant of reaction 20, 4.13×10^{-5} s^{-1} (Table 1), was determined by trial and error method by inserting the value of rate constant into model 10, with simultaneous comparison of predicted and experimentally determined values of TOC parameter and H_2O_2 concentration (Fig. 5(A) and (B)). In order to describe phenol degradation to primary by-products by UV/H_2O_2 process, model 9 was developed by upgrading model 10 with the additional set of reactions. The specific reactions for the decomposition of phenol (25–44), reaction 45 which describes catechol production due to direct photolysis of phenol and reaction 46 which describes phenol degradation to the unidentified by-products under UV irradiation, were taken into account (Fig. 5(A)). Although both mechanisms, direct photolysis and OH radicals attack, are responsible for the degradation of organic compounds by UV/H_2O_2 process, OH radicals mechanism is considered as predominant, due to the constant OH radical supply throughout H_2O_2 decomposition promoted by UV light [25,40,41]. It could be expected that the degradation of organic pollutants over direct photolysis mechanism plays a significant role only when complete amount of added hydrogen peroxide is consumed, which was not the case in this study (Fig. 5(B)). A rather good compliance of data predicted by models 9 and 10 and experimentally obtained data for all monitored species could be observed (Fig. 5(A) and (B)). It can be seen that

the efficiency of UV/H_2O_2 process for phenol degradation was significantly higher than those of UV and UV/Fe^{3+} processes, as it was expected due to the higher OH radical production. After 1 h treatment, the phenol was degraded almost completely and only 2.4% of phenol remained. At the same time the degree of partial mineralization reached the value of 14.1% removed TOC (Fig. 5(A)). The trend of the curve of phenol decomposition showed gradual leveling off, which could be contributed to the consumption of OH radicals in reactions with formed by-products (Fig. 5(A)). Again, the large difference between the sum of remaining phenol and by-products and the remained organic content expressed as TOC value can be contributed to the HAA, mostly formed by degradation of aromatic by-products: catechol, hydroquinone and benzoquinone [33].

4.3. Kinetic of dark Fenton and photo-Fenton type processes

The further modeling of dark Fenton and corresponding photo-Fenton type processes was performed on the basis of experiments conducted at established optimal operating parameters by jar test (Fig. 2).

After determining rate constants of reactions 20, 24, 45 and 46 by auxiliary models 5, 6, 7, 8, 9, and 10, the development of models 11 and 12 which describe phenol degradation by both UV/Fe^{2+}/H_2O_2 and UV/Fe^{3+}/H_2O_2 processes was approached. As it was mentioned earlier, models 1 and 2 which describe phenol degradation by Fenton process were developed as basic models. They included basic Fenton reactions, 1–16, and specific reactions for phenol decomposition to the primary by-products in model 1, 25–44, while the mineralization of phenol solution was described in model 2 by reactions 47 and 48 (Table 1). Reaction 47 describes the degradation of complete organic content of phenol solution by OH radicals to the inorganic products, i.e. CO_2 and H_2O. Due to the observed behavior of studied systems and the knowledge from the literature concerning organic pollutant degradation by Fenton type process [11–13,16] the formation of Fe^{3+}-complexes during the degradation of phenol was assumed and described by reaction 48 which was taken in account during formulation of model 2. Fe^{3+} ions tend to form organic complexes, mostly carboxylates [12], which inhibit iron regeneration cycle thus indirectly causing lack of OH radicals in the bulk. From the experimentally obtained results presented in Table 3, it can be seen that phenol and its detected primary aromatic by-products; catechol, hydroquinone and benzoquinone, are completely degraded in the first 2 min of Fe^{2+}/H_2O_2 process. Comparing those results with the experimentally obtained values of residual TOC during the treatment with the same process (Fig. 6(A)), it can be concluded that the most of organic content remained in the bulk after the second minute of process pertains to the formed aliphatic by-products, e.g. HAA, which is in agreement with the literature [12,13]. The initial drop of TOC value corresponds to the degradation of aromatics directly to CO_2 and H_2O (Table 3). Noticeable deceleration of mineralization rate after the second minute and then the achievement of steady state, 51.8% of final TOC removal (Fig. 6(A)), can be contributed to the formation of stable Fe^{3+}-complexes, i.e. precluding the catalytic cycle of iron through Fenton mechanism. This consideration corroborates the results of H_2O_2 consumption monitoring during the phenol degradation by Fe^{2+}/H_2O_2 process presented in Fig. 6(B). The same trend of TOC removal and H_2O_2 consumption can be observed. After the treatment, a relatively large amount of H_2O_2 remained in the bulk, 40.2%, confirming that iron regeneration was inhibited due to the fact that the majority of H_2O_2 consumption is related to the Fenton reactions, 1 and 2. In Table 3 and Fig. 6(A) the results of phenol degradation by UV/Fe^{2+}/H_2O_2 process are presented. Similarly like in Fe^{2+}/H_2O_2 process all detected aromatics are degraded in less than 2 min. From Fig. 6(A) which presents decrease of organic content during UV/Fe^{2+}/H_2O_2 process, it can be seen that 97.6% of phenol solution was mineralized. The plausible explanation for such high mineralization extent can be found in the fact that Fe^{3+}-complexes are destroyed under the influence of UV irradiation, thus allowing Fe^{3+} ions to participate in the Fenton catalytic cycle. Moreover, some organic acids which are the possible products of phenol oxidation, reported to be resistant to oxidation by Fenton reaction alone [42], are obviously degraded in the presence of UV light. Kavitha and Palanivelu [12] reported that carboxylic acids such as acetic and oxalic acid, identified as end products during the degradation of phenol by Fenton process, were almost completely degraded by photo-Fenton processes. Experimental results of H_2O_2 consumption monitoring presented in Fig. 6(B) speak in favor of the restitution of iron catalytic cycle. At the end of the process, maximal

Table 3
Final concentration of monitored aromatics and treatment time required for reaching that concentration by Fe^{2+}/H_2O_2 and UV/Fe^{2+}/H_2O_2 processes, comparison of experimentally obtained and predicted data by models 1 and 11

Specie		PH	CC	HQ	BQ
Fe^{2+}/H_2O_2					
Final concentration in the bulk after the treatment (mg L^{-1})	Exp.	0	0	0	0
	Model	0	0	0	0
Treatment time required for final concentration (min)	Exp.	<2	<2	<2	<2
	Model	2	2.5	2.8	3.1
UV/Fe^{2+}/H_2O_2					
Final concentration in the bulk after the treatment (mg L^{-1})	Exp.	0	0	0	0
	Model	0	0	0	0
Treatment time required for final concentration (min)	Exp.	<2	<2	<2	<2
	Model	1.2	1.5	1.4	1.9

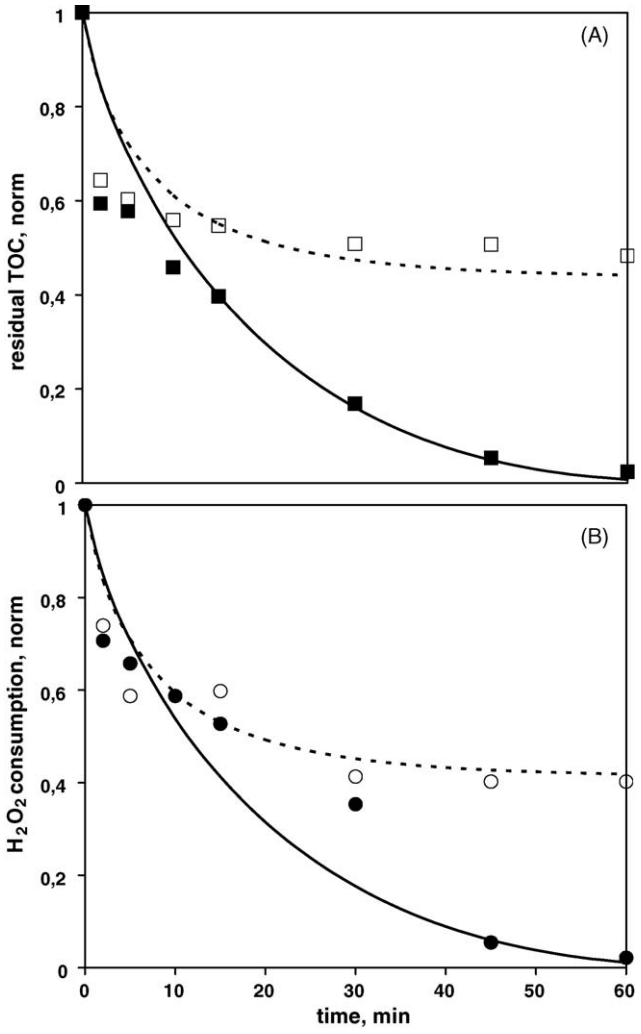

Fig. 6. Treatment of phenol solution by Fe^{2+}/H_2O_2 and UV/Fe^{2+}/H_2O_2 processes, comparison of experimental data and data predicted by developed mathematical models 11 and 12. (A) Mineralization of phenol solution. Symbols: Fe^{2+}/H_2O_2, (□) exp. and (- -) model; UV/Fe^{2+}/H_2O_2, (■) exp. and (—) model. (B) H_2O_2 consumption. Symbols: Fe^{2+}/H_2O_2, (○) exp. and (- -) model; UV/Fe^{2+}/H_2O_2, (●) exp. and (—) model.

mineralization reached 97.6% TOC removal, while only 2.2% of initial H_2O_2 remained in the bulk. It should be emphasized that considerable enhancement of Fe^{2+}/H_2O_2 process efficiency is the consequence of synergistic effect of several mechanisms. Besides the earlier described positive effect of UV irradiation on the Fenton catalytic cycle in phenol degradation, additional generation of OH radicals should be taken in account, both through direct photolysis of H_2O_2 as well as through Fe^{3+} ions reduction under UV light. However, in UV based processes organic matter could be degraded throughout both, OH radical attack and direct photolysis [25]. In Table 3 experimentally obtained data of monitored aromatics during the phenol degradation by Fe^{2+}/H_2O_2 and UV/Fe^{2+}/H_2O_2 processes are summarized, as well as those predicted by models 1 and 11. Model 11 was developed on the bases of model 1, but in accordance with the earlier discussed mechanisms involved in phenol degradation by UV/Fe^{2+}/H_2O_2 process, additional reactions 20, 24, 45 and 46 were taken into account. Validity of models 1 and 11 was estimated on the basis of treatment time required for reaching the final concentration of monitored species in the bulk, due to the complete degradation of aromatics prior to the second minute of treatment by both processes, when first aliquot was taken from reaction mixture for HPLC and TOC analyses. Negligible delay in prediction of model 1 for phenol degradation by Fe^{2+}/H_2O_2 process can be observed, while the predicted treatment time required for the disappearance of monitored aromatics by model 11 is less than 2 min, as it was determined experimentally. In Fig. 6(A) and (B) the comparison of experimental and predicted data by model 2, for TOC removal and H_2O_2 consumption during the phenol degradation by Fe^{2+}/H_2O_2 process is presented. The value of rate constant of reaction 47, $2.33 \times 10^8\ M^{-1}\ s^{-1}$, was determined by trial and error method fitting the values into model 2 with simultaneous comparison of predicted and experimentally determined values of both monitored parameters. Similarly like in the case of models 1 and 11, model 12 which describes mineralization of phenol solution by UV/Fe^{2+}/H_2O_2 process was developed on the basis of model 2, where additional reactions 20, 24, 49 and 50 were included in model formulation. Reaction 49 describes decomposition of Fe^{3+}-complexes under UV irradiation, and its value of rate constant, $1 \times 10^{-3}\ s^{-1}$, was determined by trial and error method fitting the values into model 12. Good accordance of data predicted by the developed models 2

Table 4
Final concentration of monitored aromatics and treatment time required for reaching that concentration by Fe^{3+}/H_2O_2 and UV/Fe^{3+}/H_2O_2 processes, comparison of experimentally obtained and predicted data by models 1 and 11

Specie		PH	CC	HQ	BQ
Fe^{3+}/H_2O_2					
Final concentration in the bulk after the treatment ($mg\ L^{-1}$)	Exp.	0	0	0	0
	Model	0	0	0	0
Treatment time required for final concentration (min)	Exp.	2–15	<2	<2	2–15
	Model	3.4	4.0	4.2	4.7
UV/Fe^{3+}/H_2O_2					
Final concentration in the bulk after the treatment ($mg\ L^{-1}$)	Exp.	0	0	0	0
	Model	0	0	0	0
Treatment time required for final concentration (min)	Exp.	<2	<2	<2	<2
	Model	2.0	3.1	3.2	3.6

and 12 and those experimentally obtained for TOC removal and H_2O_2 consumption can be observed. The exception is H_2O_2 profile observed in the time interval 15–45 min of UV/Fe^{2+}/H_2O_2 process, where lower consumption of H_2O_2 was determined experimentally than that predicted by model 12.

In Table 4 and Fig. 7(A) and (B) results of phenol degradation by Fe^{3+}/H_2O_2 and UV/Fe^{3+}/H_2O_2 processes are presented. Models 1, 2, 11 and 12 were used to describe degradation kinetics of phenol solution. Although complete degradation of aromatics was accomplished by Fe^{3+}/H_2O_2 and UV/Fe^{3+}/H_2O_2 processes, it can be seen that Fe^{3+}/H_2O_2 process is somewhat slower than the process which involves Fe^{2+} salt (Tables 3 and 4). Similarly like in the case of Fe^{2+}/H_2O_2 process, a small delay in the predicted treatment time required for reaching final concentration of aromatics in phenol solution by Fe^{3+}/H_2O_2 and UV/Fe^{3+}/H_2O_2 processes is observed (models 1 and 11). From Fig. 7(A) and (B) it can be seen that models 2 and 12 successfully describe both mineralization of phenol solution and H_2O_2 consumption by Fe^{3+}/H_2O_2 and UV/Fe^{3+}/H_2O_2 processes. Fe^{3+}/H_2O_2 process efficiency was enhanced by the presence of UV irradiation from 55.3% up to 97.2% of TOC removal, which was followed by a correspondingly larger consumption of H_2O_2.

Table 5 and Fig. 8(A) and (B) present results of phenol degradation by Fe^0/H_2O_2 and UV/Fe^0/H_2O_2 processes. From Table 5 it can be seen that the complete degradation of phenol and detected aromatic by-products; catechol, hydroquinone and benzoquinone, was achieved by Fenton type processes using iron powder similarly like in those utilizing iron salts. However, it should be emphasized that the degradation of aromatics by Fe^0/H_2O_2 and UV/Fe^0/H_2O_2 processes is relatively slower. After the second minute of treatment by Fenton type processes using iron salts neither phenol nor its aromatic by-products were detected in the bulk, while in the case of Fe^0/H_2O_2 and UV/Fe^0/H_2O_2 processes, the disappearance of aromatics was observed after 45 and 30 min, respectively. Similar effect can be observed from Fig. 8(A) where the results of mineralization of phenol solution by both processes with iron powder as a source of catalytic iron are presented. A relatively equable decrease of TOC value to the achievement of final mineralization extent, 39.8% TOC removal, can be observed (Fig. 8(A)). This trend significantly differs from those observed by Fe^{2+}/H_2O_2 and Fe^{3+}/H_2O_2 processes (Figs. 6(A) and 7(A)) where after the

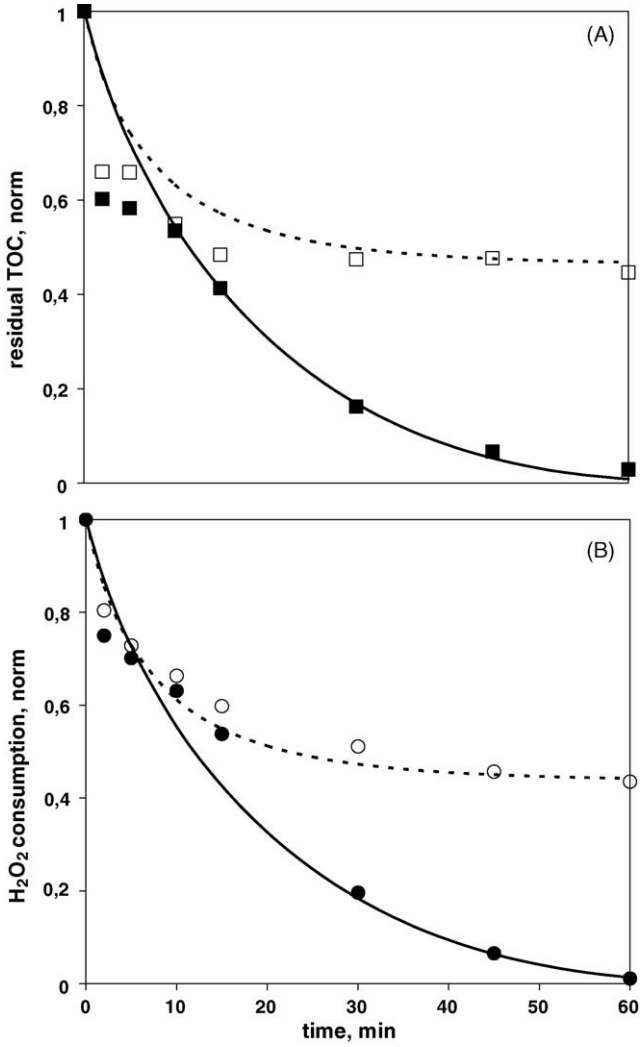

Fig. 7. Treatment of phenol solution by Fe^{3+}/H_2O_2 and UV/Fe^{3+}/H_2O_2 processes, comparison of experimental data and data predicted by developed mathematical models 11 and 12. (A) Mineralization of phenol solution. Symbols: Fe^{3+}/H_2O_2, (□) exp. and (- -) model; UV/Fe^{3+}/H_2O_2, (■) exp. and (—) model. (B) H_2O_2 consumption. Symbols: Fe^{3+}/H_2O_2, (◯) exp. and (- -) model; UV/Fe^{3+}/H_2O_2, (●) exp. and (—) model.

Table 5
Final concentration of monitored aromatics and treatment time required for reaching that concentration by Fe^0/H_2O_2 and UV/Fe^0/H_2O_2 processes, comparison of experimentally obtained and predicted data by models 3 and 13

Specie		PH	CC	HQ	BQ
Fe^0/H_2O_2					
Final concentration in the bulk after the treatment (mg L^{-1})	Exp.	0	0	0	0
	Model	0	0	0	0
Treatment time required for final concentration (min)	Exp.	30–45	30–45	0	30–45
	Model	47.2	48.5	0	52.9
UV/Fe^0/H_2O_2					
Final concentration in the bulk after the treatment (mg L^{-1})	Exp.	0	0	0	0
	Model	0	0	0	0
Treatment time required for final concentration (min)	Exp.	15–30	15–30	0	15–30
	Model	35.6	38.2	0	41.3

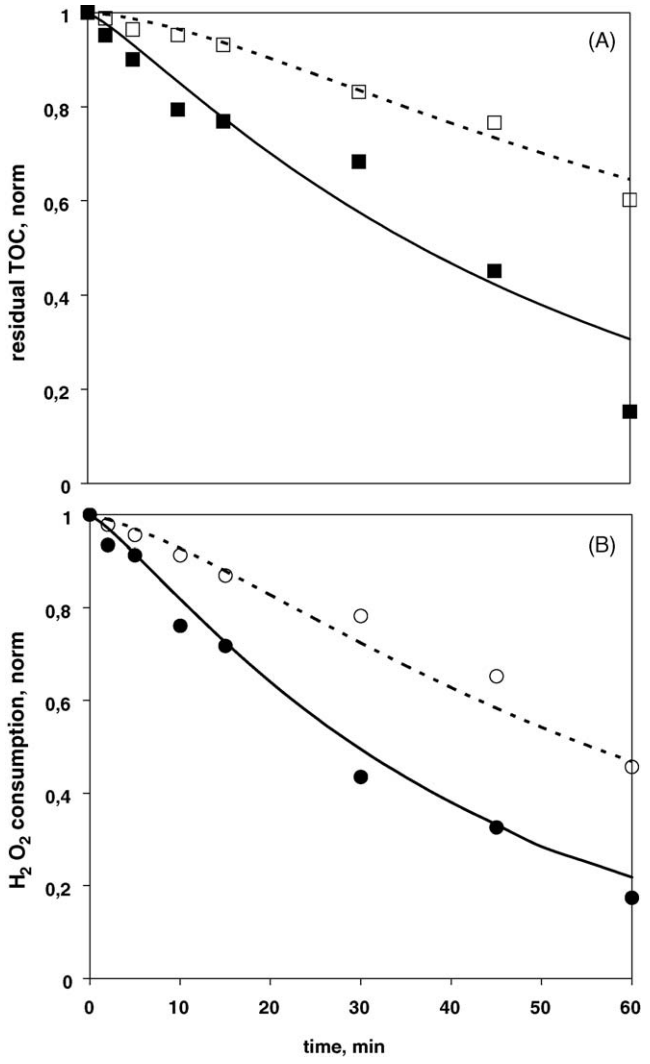

Fig. 8. Treatment of phenol solution by Fe^0/H_2O_2 and $UV/Fe^0/H_2O_2$ processes, comparison of experimental data and data predicted by developed mathematical models 13 and 14. (A) Mineralization of phenol solution. Symbols: Fe^0/H_2O_2, (□) exp. and (- -) model; $UV/Fe^0/H_2O_2$, (■) exp. and (—) model. (B) H_2O_2 consumption. Symbols: Fe^0/H_2O_2, (○) exp. and (- -) model; $UV/Fe^0/H_2O_2$, (●) exp. and (—) model.

initial drop of TOC, oxidation process was inhibited by formation of Fe^{3+}-complexes. Evidently, due to slow leaching of ions from iron powder surface, constant supply of Fe^{2+} ions necessary for continuous OH radicals production throughout the Fenton mechanism is ensured [31]. Also, low concentration of Fe^{3+} species in the bulk does not favor formation of stable complexes with aliphatic phenol by-products. In order to describe Fe^0/H_2O_2 and $UV/Fe^0/H_2O_2$ processes, reactions involving iron powder should be incorporated into the model formulation. Bergendahl and Thies [23] assumed that Fe^0 was oxidized only directly into the bulk Fe^{2+} ions throughout reaction with hydrogen peroxide, 19. However, on the basis of experimental results obtained in this study and observation of other authors [31,43] it was concluded that describing of the leaching mechanism of iron ions from the iron powder surface given by simple reaction 19 should be extended with additional reactions. Therefore, the formation of Fe^{2+} surface ions which are able to react with H_2O_2 thus generating OH radicals was assumed, 17 and 18. Prediction of phenol degradation by Fe^0/H_2O_2 process was provided by model 4 which was developed by including additional reactions 17–19 (Table 1) into model 2. Rate constants for reactions 17–19 were determined by trial and error method fitting the values into model 4 with simultaneous comparison of predicted and experimentally obtained values of TOC and H_2O_2 concentration (Fig. 8(A) and (B)) as well as final concentration of Fe^{2+}/Fe^{3+} ions in the bulk (Table 6). Trend of H_2O_2 consumption by Fe^0/H_2O_2 process followed the decreasing of TOC value. After 1 h treatment, 45.7% of initial H_2O_2 concentration remained in the reaction mixture. For both monitored parameters during the treatment of phenol solution by Fe^0/H_2O_2 process a good accordance of predicted (model 4) and experimentally obtained values can be observed (Fig. 8(A) and (B)). Similar like in the case of model 1 for prediction of phenol decomposition to the detected aromatic by-products by Fe^{2+}/H_2O_2 and Fe^{3+}/H_2O_2 processes, model 3 predicts treatment time required for reaching final concentration of aromatics in phenol solution with certain delay in comparison to experimentally obtained data (Table 5). This can be explained by a possible positive effect of solid particles on the efficiency of AOPs reported by several authors [44–47]. This type of interaction was not considered during the model formulation. Enhancement of Fe^0/H_2O_2 process by UV irradiation, manifested in the shorter treatment time required for complete degradation of aromatics in phenol solution (Table 5) as well as in the significant decrease of residual TOC, 15.2%, associated with the increase of H_2O_2 consumption (Fig. 8(A) and (B)). Model 4 was upgraded with additional reactions concerning UV irradiation, 20, 24, 49 and 50 (Table 1), to give model 14 for the prediction of mineralization of phenol solution by $UV/Fe^0/H_2O_2$ process. Certain discrepancy between experimental and predicted TOC values (Fig. 8(A)) can be contributed to the effect of solid particles, iron powder, that was not included in the model formulation, as mentioned above. On the other hand, a good accordance in the case of H_2O_2 consumption can be observed from Fig. 8(B). The prediction of phenol decomposition to the detected aromatic by-products by $UV/Fe^0/H_2O_2$ process was described by model 13 which was developed from model 3 in the same manner as model 14 from model 4. From Table 5 it can be seen that model 13 predicts treatment time required for reaching complete degradation of aromatics in phenol solution with certain delay in comparison to experimentally obtained data, presumably due to the same assumption given as the explanation for model 3.

Table 6
Comparison of processes regarding mineralization efficiency and Fe^{2+} and Fe^{3+} ions concentration in the bulk after the treatment

Process	Total concentration of Fe ions after the treatment (mM)	Residual TOC (%)
Fe^{2+}/H_2O_2	1.0	48.2
Fe^{3+}/H_2O_2	1.0	44.3
Fe^0/H_2O_2	0.77	60.2
$UV/Fe^{2+}/H_2O_2$	1.0	2.4
$UV/Fe^{3+}/H_2O_2$	1.0	2.8
$UV/Fe^0/H_2O_2$	0.35	15.2

Table 6 summarizes values of residual TOC and Fe^{2+}/Fe^{3+} ions concentration in the bulk after the treatment by Fenton type processes, Fe^{2+}/H_2O_2, Fe^{3+}/H_2O_2, Fe^0/H_2O_2, $UV/Fe^{2+}/H_2O_2$, $UV/Fe^{3+}/H_2O_2$ and $UV/Fe^0/H_2O_2$. It can be seen that concerning TOC removal, $UV/Fe^{2+}/H_2O_2$ and $UV/Fe^{3+}/H_2O_2$ processes are the most efficient among all studied systems. Although efficiency of processes utilizing Fe^0 as a source of iron catalyst was somewhat lower than corresponding homogeneous Fenton type processes, benefits from the environmental and economical point of view, due to the quality of treated water, should not be ignored. Significantly lower concentration of Fe^{2+} and Fe^{3+} ions in the bulk after the treatment, particularly by $UV/Fe^0/H_2O_2$ process with only 0.35 mM of iron ions and relatively low amount of residual TOC, 15.2%, in comparison to homogeneous Fenton type processes can be observed (Table 6). Such results were expected due to knowledge from the literature that the amount of iron ions can be reduced up to 50% using iron powder instead of iron salts as a source for iron catalysts [48]. Moreover, by utilization of iron powder, the contamination of treated solution with unnecessary counter-ions is avoided, thus lowering overall costs of wastewater treatment.

5. Conclusions

Fenton type, Fe^{2+}/H_2O_2, Fe^{3+}/H_2O_2 and Fe^0/H_2O_2, and corresponding photo-assisted processes, $UV/Fe^{2+}/H_2O_2$, $UV/Fe^{3+}/H_2O_2$ and $UV/Fe^0/H_2O_2$, were successfully applied for the treatment of phenol solution. Although complete degradation of phenol and its primary oxidation by-products, catechol, hydroquinone and benzoquinone, was achieved, mineralization extents ranged from 39.8 to 97.6% of removed TOC in the increasing order $Fe^0/H_2O_2 < Fe^{2+}/H_2O_2 < Fe^{3+}/H_2O_2 < UV/Fe^0/H_2O_2 < UV/Fe^{3+}/H_2O_2 < UV/Fe^{2+}/H_2O_2$. Models to describe phenol degradation by all applied processes were developed. With the exception of models for phenol degradation by processes including solid particles, iron powder, developed models closely predict the behavior of investigated systems. The proposed models appeared to adequately represent the key mechanisms and kinetics of phenol oxidation by investigated AOPs.

Acknowledgement

Financial support from the Ministry of Education, Science, and Sport (Croatia) (project #0125–018) are gratefully acknowledged.

References

[1] Z. He, J. Liu, W. Cai, The important role of the hydroxy ion in phenol removal using pulsed corona discharge, J. Electrostat. 63 (5) (2005) 371–386.
[2] R. Alnaizy, A. Akgerman, Advanced oxidation of phenolic compounds, Adv. Environ. Res. 4 (3) (2000) 233–244.
[3] U.S. Environmental Protection Agency, Toxicological review of phenol, EPA/635/R-02/006, In support of summary information on the integrated risk information system (IRIS), 2002.
[4] A.P. Sincero, G.A. Sincero, Physical-Chemical Treatment of Water and Wastewater, CRC Press, IWA Publishing, New York, USA, 2003.
[5] R.J. Droste, Theory and Practice of Water and Wastewater Treatment, John Wiley and Sons, New York, USA, 1997.
[6] M.D. La Grega, P.L. Buckingham, J.C. Evans, Hazardous Waste Management, McGraw-Hill, New York, USA, 1994.
[7] N. Daneshvar, D. Salari, A.R. Khataee, Photocatalytic degradation of azo dye Acid Red 14 in water: investigation of the effect of operational parameters, J. Photochem. Photobiol. A 157 (2003) 111–116.
[8] P.R. Gogate, A.B. Pandit, A review of imperative technologies for wastewater treatment. I. Oxidation technologies at ambient conditions, Adv. Environ. Res. 8 (2004) 501–551.
[9] P.R. Gogate, A.B. Pandit, A review of imperative technologies for wastewater treatment. II. Hybrid methods, Adv. Environ. Res. 8 (2004) 553–597.
[10] P. Lukes, Water Treatment by pulsed streamer corona discharge, Institute of Plasma Physics ASCR, Prague, Czech Republic, 2001.
[11] M.A. Tarr, Fenton and modified Fenton methods for pollutant degradation, in: M.A. Tarr (Ed.), Chemical degradation methods for wastes and pollutants – environmental and industrial applications, Marcel Dekker Inc., New York, USA, 2003, pp. 165–200.
[12] V. Kavitha, K. Palanivelu, The role of ferrous ion in Fenton and photo-Fenton processes for the degradation of phenol, Chemosphere 55 (2004) 1235–1243.
[13] R. Maciel, G.L. Sant'Anna Jr., M. Dezotti, Phenol removal from high salinity effluents using Fenton's reagent and photo-Fenton reactions, Chemosphere 57 (2004) 711–719.
[14] S. Esplugas, J. Gimenez, S. Contreras, E. Pascual, M. Rodriguez, Comparison of different Advanced Oxidation Processes for phenol degradation, Water Res. 36 (2002) 1034–1042.
[15] R. Chen, J.J. Pignatello, Role of quinone intermediates as electron shuttles in Fenton and photoassisted Fenton oxidations of aromatic compounds, Environ. Sci. Technol. 31 (1997) 2399–2406.
[16] N. Kang, D.S. Lee, J. Yoon, Kinetic modeling of Fenton oxidation of phenol and monochlorophenols, Chemosphere 47 (2002) 915–924.
[17] H.J. Kuhn, S.E. Braslavsky, R. Schmidt, Chemical actinometry, IUPAC technical report, Pure Appl. Chem. 76 (12) (2004) 2105–2146.
[18] L.S. Clesceri, A.E. Greenberg, A.D. Eaton, Standard Methods for the Examination of Water and Wastewater Treatment, 20th ed., APHA and AWWA and WEF, USA, 1998.
[19] A.A. Burbano, D.D. Dionysiou, M.T. Suidan, T.L. Richardson, Oxidation kinetics and effect of pH on the degradation of MTBE with Fenton reagent, Water Res. 39 (2005) 107–118.
[20] H. Gallard, J. De Laat, Kinetic modelling of $Fe(III)/H_2O_2$ oxidation reactions in dilute aqueous solution using atrazine as a model organic compound, Water Res. 34 (12) (2000) 3107–3116.
[21] D.R. Grymonpre, A.K. Sharma, W.C. Finney, B.R. Locke, The role of Fenton's reaction in aqueous phase pulsed streamer corona reactors, Chem. Eng. J. 82 (1–3) (2001) 189–207.
[22] D.R. Grymonpre, W.C. Finney, R.J. Clark, B.R. Locke, Suspended activated carbon particles and ozone formation in aqueous phase pulsed corona discharge reactors, Ind. Eng. Chem. Res. 42 (2003) 5117–5134.
[23] J.A. Bergendahl, T.P. Thies, Fenton's oxidation of MTBE with zero-valent iron, Water Res. 38 (2004) 327–334.
[24] J.C. Crittenden, S. Hu, D.W. Hand, S.A. Green, A kinetic model for H_2O_2/UV process in a completely mixed batch reactor, Water Res. 33 (10) (1999) 2315–2328.
[25] F.J. Beltran, Ozone-UV radiation-hydrogen peroxide oxidation technologies, in: M.A. Tarr (Ed.), Chemical Degradation Methods for Wastes and Pollutants – Environmental and Industrial Applications, Marcel Dekker Inc., New York, USA, 2003, pp. 1–77.
[26] M. Rodríguez, N.B. Abderrazik, S. Contreras, E. Chamarro, J. Gimenez, S. Esplugas, Iron(III) photoxidation of organic compounds in aqueous solutions, Appl. Catal. B 37 (2) (2002) 131–137.
[27] O. Gimeno, M. Carbajo, F.J. Beltran, F.J. Rivas, Phenol and substituted phenols AOPs remediation, J. Hazard. Mater. B 119 (2005) 99–108.
[28] N. Nirmalakhandan, Modeling Tools for Environmental Engineers and Scientists, CRC Press, New York, USA, 2002.
[29] http://www.h202.com.

[30] H. Kusic, A. Lonacaric Bozic, N. Koprivanac, Fenton type processes for minimization of organic content in coloured wastewaters. Part I. Processes optimization, Dyes Pigm., in press.
[31] W.Z. Tang, R.Z. Chen, Decolorization kinetics and mechanism of commercial dyes by H_2O_2/iron powder system, Chemosphere 32 (5) (1996) 947–958.
[32] P.W. Atkins, Physical Chemistry, 5th ed., Oxford University Press, Oxford, UK, 1994.
[33] B. Roig, C. Gonzalez, O. Thomas, Monitoring of phenol photodegradation by ultraviolet spectroscopy, Spectrochim. Acta, Part A 59 (2) (2003) 303–307.
[34] P. Lukes, B.R. Locke, Degradation of substituted phenols in hybrid gas–liquid electrical discharge reactor, Ind. Eng. Chem. Res. 44 (9) (2005) 2921–2930.
[35] M. Neamtu, A. Yediler, I. Siminiceanu, A. Kettrup, Oxidation of commercial reactive azo dye aqueous solutions by photo-Fenton and Fenton-like processes, J. Photochem. Photobiol. A 161 (2003) 87–93.
[36] D. Zhou, F. Wu, N. Deng, W. Xiang, Photooxidation of bisphenol A (BPA) in water in the presence of ferric and carboxylate salts, Water Res. 38 (19) (2004) 4107–4116.
[37] M.I. Franch, J.A. Ayllón, J. Peral, X. Domènech, Fe(III) photocatalyzed degradation of low chain carboxylic acids: implications of the iron salt, Appl. Catal. B 50 (2) (2004) 89–99.
[38] R. Andreozzi, R. Marotta, Removal of benzoic acid in aqueous solution by Fe(III) homogeneous photocatalysis, Water Res. 38 (5) (2004) 1225–1236.
[39] B.D. McGinnis, V.D. Adams, E.J. Middlebrooks, Degradation of ethylene glycol in photo Fenton systems, Water Res. 34 (8) (2000) 2346–2354.
[40] Y.-S. Shen, D.-K. Wang, Development of photoreactor design equation for the treatment of dye wastewater by UV/H_2O_2 process, J. Hazard. Mater. B 89 (2002) 267–277.
[41] A. Aleboyeh, Y. Moussa, H. Aleboyeh, Kinetics of oxidative decolourisation of Acid Orange 7 in water by ultraviolet radiation in the presence of hydrogen peroxide, Sep. Purif. Technol. 43 (2) (2005) 143–148.
[42] R.J. Bigda, Consider Fenton's chemistry for wastewater treatment, Chem. Eng. Prog. 91 (1995) 62–66.
[43] P.G. Tratnyek, Permeable reactive barriers of iron and other zero-valent metals, in: M.A. Tarr (Ed.), Chemical Degradation Methods for Wastes and Pollutants – Environmental and Industrial Applications, Marcel Dekker Inc., New York, USA, 2003, pp. 371–422.
[44] R.D. Vidic, M.T. Suidan, R.C. Brenner, Oxidative coupling of phenols on activated carbon: impact on adsorption equilibrium, Environ. Sci. Technol. 27 (1993) 2079–2085.
[45] N.S. Abuzaid, G.F. Nakhla, Dissolved oxygen effects on equilibrium and kinetics of phenolics adsorption by activated carbon, Environ. Sci. Technol. 28 (1994) 210–221.
[46] D.R. Grymonpre, W.C. Finney, B.R. Locke, Activated carbon particles in aqueous phase pulsed streamer corona discharge, J. Adv. Oxid. Technol. 4 (1999) 408–416.
[47] H. Kusic, N. Koprivanac, I. Peternel, B.R. Locke, Hybrid gas/liquid electrical discharge reactors with zeolites for colored wastewater degradation, J. Adv. Oxid. Technol. 8 (2005) 172–181.
[48] F. Lücking, H. Köser, M. Jank, A. Ritter, Iron powder, grafite and activated carbon as catalysts fir the oxidation of 4-chlorophenol with hydrogen peroxide in aqueous solution, Water Res. 32 (1998) 2607–2614.